Conference Paper, Published Version

Baranya, Sandor; Józsa, J.; Napoli, E.

Field and numerical study of river confluence flow structures

River Flow 2010 - Dittrich, Koll, Aberle & Geisenhainer (eds) - © 2010 Bundesanstalt für Wasserbau ISBN 978-3-939230-00-7

Field and numerical study of river confluence flow structures

S. Baranya & J. Józsa
Department of Hydraulic and Water Resources Engineering, Budapest University of Technology and Economics, Budapest, Hungary

E. Napoli
Department of Hydraulic and Environmental Engineering, University of Palermo, Palermo, Italy

ABSTRACT: The confluence zone of two moderate size rivers (mean discharge around 50 m^3/s each) in Hungary was chosen to investigate three-dimensional flow structures typical to such zones. Two field survey campaigns were carried out using up-to-date ADCP technology. Measurements were done by applying two methods: moving boat with systematic, continuous crossings on one hand, and in stationary mode in selected verticals, on the other hand. The former offered an overall, though locally instantaneous, spatial velocity field, whereas the latter resulted in local time-averaged velocity profiles. Helical flow structures of the confluence zone were shown by representing secondary current strengths and orientation in a vector form. In parallel, first a three-dimensional RANS flow model was also used to reproduce the essential of the spatial flow structure. Model validation was accomplished by comparing calculated velocity fields with measured ones, moreover, the above mentioned vectors quantifying the secondary currents were also looked at. Besides steady-state RANS modeling, attempts were made to capture the space-time behavior also on a LES modeling-basis, focusing on the reasonable reproduction of the rather complex vortical motion in the post-confluence channel reach, as a possible combination of vortex shedding at the blunt tip of the confluence and shear layer instabilities turning to Kelvin-Helmholtz type of vortex formation at the interface zone of the two rivers, all this besides the developing helical flow components.

Keywords: Confluence zone, ADCP, CFD modeling, RANS, LES

1 INTRODUCTION

Exploring space-time flow structures and reproducing them by numerical modeling in river confluence zones is still a challenging task in hydraulic research and engineering. Fortunately, rivers carrying suspended solids different in color make visible these features on the surface as one can find at a lot of confluences, see e.g. the joining of three rivers at Passau in Germany or the fascinating pattern developed at the junction of Thomson and Fraser rivers in Canada. However, the development mechanism, the role of various 2- and 3D coherent structures, the generation of helical flow components need significant research efforts. In doing so, field measurements can provide valuable information and straightforward validation data to advanced numerical models, which can be then used to study even details hardly measurable.

Recently, several articles have dealt with river-confluence zones and presented field and laboratory measurements as well as two- and three-dimensional numerical simulations. As to the field measurements Rhoads and Sukhodolov (2001a) examined the three-dimensional time averaged flow structure at three confluences using Acoustic Doppler Velocimeter (ADV). They introduced, in one of the three sites, that helical motion can be a characteristic feature of confluence flow structure. It was shown that two surface-convergent helical cells exist within the confluence and that the dual cell structure transforms into a single-cell structure as flow enters the downstream channel. By postprocessing ADV velocity data turbulence characteristics were quantified (Rhoads and Sukhodolov, 2001b). They showed that the developed shear layer in the confluence zone generates higher turbulence, however, the intense turbulence does not appear to be highly effective at mixing the two flows. De Serres *et al.* (1999) collected three-dimensional data of the mean and turbulent structure of flow at a river confluence and illustrated how these features vary in relation with changes in bed morphology and fluctuations in the

ratio of momentum flux between the confluent rivers. It was shown that both relative difference of depth between the two streams and momentum ratio have a strong effect on the flow structure.

To study the hydrodynamically complex flow features in confluence zones several numerical simulations were carried out, though in very few cases together with laboratory and/or field measurements. Biron *et al.* (2004) studied mixing processes in laboratory and field confluences applying a 3D RNG k-ε turbulence model called PHOENICS (RNG refers to the Re-normalisation Group Theory discussed, for example, in Pope, 2001). They commented on the difference between concordant (i.e. equal in both rivers) and discordant (conversely, uneven) bed levels. They also reported that planform curvature of the channels affects mixing and underlined the role of bed level differences between the two channels, as well. It was shown that in case of discordant bed the mixing process is much faster. Effect of the junction angle was also investigated and it was shown that at higher angles, mixing is more rapid.

The main purpose of this paper is to study the nature of hydrodynamics in a complex way with the mentioned methods fixed-boat ADCP measurements as well as Reynolds Averaged (RANS) and Large Eddy Simulation (LES) modeling approaches.

2 FIELD SURVEYS

2.1 *Study site*

In this study the junction of two rivers in the urban area of Győr in north-western Hungary, was chosen and investigated in detail (Fig. 1). Here, the main stream is a regulated secondary branch of the River Danube, known as Mosoni-Duna, with a mean flow of around 50 m³/s rather constant over the year, that can be, however, affected by significant backwater when the Danube floods. The second stream is the River Rába with a similar mean discharge that, in contrast, can rise to several hundred cubic meters per second in flood events owing to a catchment area nearly as large as 10,000 km².

For this study, river bed geometry was surveyed using an ultrasonic depth sounder. Measurements were carried out in cross-sections with an average spacing of 20 m apart.

2.2 *Fixed boat measurements*

For the flow measurements an RDI four beam 600 kHz Rio Grande ADCP, vertically down looking, was deployed from a vessel. A sampling frequency of 3 Hz, with a vertical space resolution of 10 cm was used. The main goal was to detect the swirling character of flow, pointing out the deviation of flow velocity vectors along the verticals. Most likely, such flow structures can not be evaluated from typical moving boat measurements, where instantaneous velocities show strong scattering due to turbulence motion. Therefore, 13 points were chosen downstream of the junction, where long-term velocity measurements were done.

During the measurement campaign the river discharges were Q_{MD}=65 m^3/s, $Q_{Rába}$=75 m^3/s, respectively. From the survey time averaged velocities were derived and plotted. Due to the bends of upstream channels swirling flow structures are developing as the flow approaches the confluence. The phenomenon can also be called helical flow, which can be explained with the accumulated effects of primary and secondary flows. Reaching the junction the two swirling flows are joining each other and a two-cell helical motion is developing here. Figure 2 shows time averaged velocities confirming the mentioned behavior of the flows.

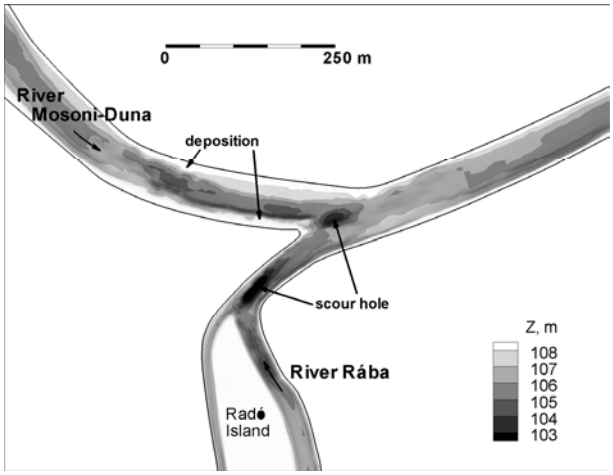

Figure 1. Topography of the studied river confluence.

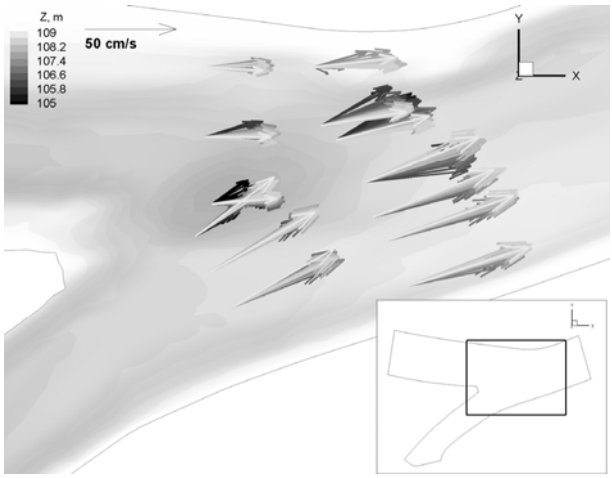

Figure 2. Plan view of time averaged velocity vectors (grayscale indicates vector location in the vertical; black vectors: close to river bed, white vectors: close to free surface).

For the characterization of the strength of secondary current a circulation vector (**S**) was defined, which can be calculated for each profile (Fig. 3). It is created based on the difference vector between the flow velocities closest to the water surface ($\mathbf{u}_{top}$) and to the river bottom ($\mathbf{u}_{bed}$). This difference vector is projected onto the plane perpendicular to the direction of depth averaged flow ($\mathbf{u}_{av}$), then rotated with 90° clockwise or anticlockwise depending on the sense of helical motion (according to a left-handed system). Since ADCP measures three-dimensional velocity, depth averaged velocities presented represent the total velocity vector.

According to Stokes theorem the resulted vector represents the circulation per unit width. The horizontal components of the circulation vector of the secondary currents can be derived from the following formula:

$$S_X = \frac{U_{av}}{|\mathbf{u}_{av}|}\left|\mathbf{u}_{top} - \mathbf{u}_{bed}\right| c \sin(\delta - \varepsilon)$$

$$S_Y = \frac{V_{av}}{|\mathbf{u}_{av}|}\left|\mathbf{u}_{top} - \mathbf{u}_{bed}\right| c \sin(\delta - \varepsilon)$$

$$c = \mathrm{sign}(\varphi_{top} - \varphi_{bed})$$

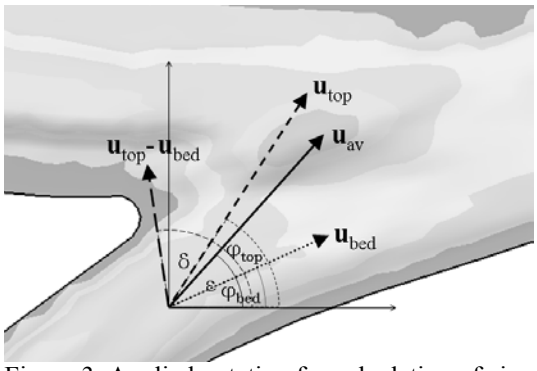

Figure 3. Applied notation for calculation of circulation vector.

Helical flow structure was studied plotting the above defined secondary current vectors from two different measurement campaigns (Fig. 4) Vectors pointing in the flow direction mean a swirling character of clockwise direction, looking at a cross-section from downstream. As expected the discharge ratio of the rivers determines the extension of helical cells, i.e. the secondary flow developing from the higher discharge will represent larger areas in the confluence zone. Strongest swirling characters arise in the shear layer, which may probably be the complex effect of the characteristic flow pattern in river curvatures, and the interaction between flow and scour hole development. As to the characteristic flow pattern in river curvatures, it can be stated that the basic flow structure in a river bend shows a helical motion. Flow close to free surface moves toward the outer bank because of centripetal acceleration, whereas near-bed flow tends to the direction of inner bank.

Additionally, it is also shown that in natural bends this helical motion is present only in the outer part of the river in case of a point bar development at the inner bank. The interaction between flow and scour hole development was explained by Bradbrook *et al.* (2000). They pointed out the steering effect of bed topography marking the difference in flow structure between flat bed and real bed geometry. As the flow interacts with the scour hole a strong downwelling zone appears in the shear layer enhancing secondary circulation, as was found here.

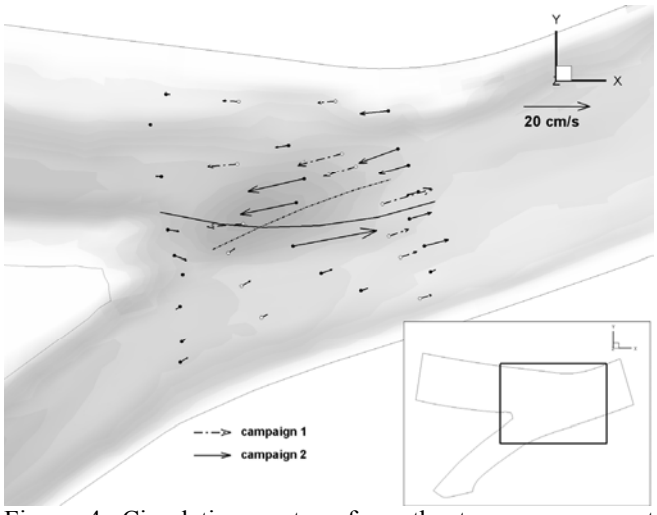

Figure 4. Circulation vectors from the two measurement campaigns.

3 RANS MODELING

3.1 *Solver*

The numerical tool exploited in this study is the CFD code called SSIIM, which stands for Sediment Simulation In Intakes with Multiblock option (Olsen, 2002).

SSIIM solves the 3D RANS equations with the *k*-ε turbulence closure (see *e.g.* Pope, 2001) by using a finite-volume method and the SIMPLE algorithm (Patankar, 1980) on a three-dimensional, non-orthogonal, structured grid. The momentum equations are in complete form, without resorting to the hydrostatic assumption.

Dirichlet boundary conditions have to be assigned at the inflow boundary. At the outflow boundaries, zero-gradient conditions are used for all variables. On the bed the velocity profile is calculated from the well-known formula (Schlichting, 1979):

$$U = \frac{u_*}{\kappa} \ln \frac{30z}{k_s}$$

where U is boundary aligned velocity, u_* is friction or bed shear velocity, κ is von Karman constant (0.41), z is distance from the wall and k_s is the Nikuradze roughness. At the water surface, U_x, U_y, P and ε have zero gradient boundary conditions, whereas U_z is set to a certain value and k is equal to zero.

3.2 *The numerical domain*

The rivers' elevation model was mapped onto a single-block structured grid fitted to the banks with 150 streamwise and 48 spanwise cells, corresponding to an average cell size of 6x3 m. A limited number of cells were blocked out to represent land areas. Vertically, 10 cell layers were used refined toward the bottom so as to capture strong gradients. Overall, there were approximately 70000 active cells.

3.3 *Results*

The main purpose of numerical investigations was to see the feasibility of reproduction of spatial flow structures and to gain a better knowledge on the nature of confluence flows. RANS modeling results show significant spatial behavior of confluence flow. Due to river curvatures a helical motion develops connecting to and enhancing each other in the post-confluence channel. This mechanism is similar to the flow pattern in a river bend and can be explained with the interaction between centripetal acceleration and the counteracting pressure gradient force.

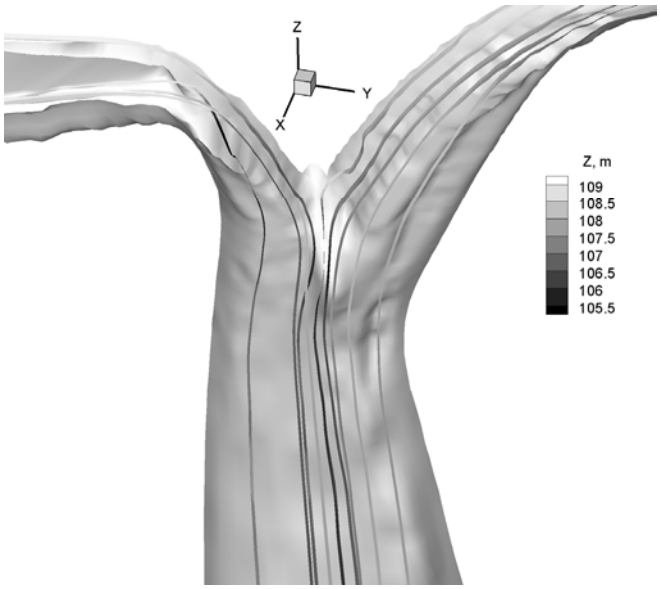

Figure 5. Stream-traces colored by elevation in the confluence zone (Perspective view).

Two counter-rotating secondary circulations result in a considerable downwelling at junction apex as it can be seen from Figure 5, where stream-traces starting from free surface close to inner banks are moving toward the river bottom, while the ones from outer banks are concentrating in the confluence centerline. Since strong helical motion is present only from the apex to a distance of approximately one river width, stream-traces that got to river bed due to downwelling are remaining in that horizontal layer. Although, it was also shown that post-confluence channel planform and bed topography also influence the flow structure, as a strong one-cell swirling flow develops owing to significant sediment deposition on right bank and low-radius bank curvature at left side.

4 LARGE EDDY SIMULATION OF THE FLOW FIELD

4.1 *Numerical model and simulation setup*

The results of the field experiments analyzed in the previous section clearly show the high complexity of the flow field downstream of the river confluence. Further insight on the highly three-dimensional flow patterns can be obtained through a numerical analysis, resolving the free-surface mass and momentum equations.

Although the *statistical approach* based on the solution of the RANS allows to obtain a complete description of the time-averaged flow field, it is well known that RANS results frequently show a somewhat poor agreement with experimental data in problems characterized by strong secondary currents. An example of this is given in the recent paper of Miyawaki *et al.* (2009), focused on a river confluence problem. In the paper the authors show that the streamwise-oriented helical cells predicted by RANS solutions are not strong enough to capture the presence of two zones of high velocity in the cross-section, as obtained in field experiments.

On the other side, in meandering flows in compound cross-sections RANS solutions were obtained using standard k-ε turbulence modeling that exhibited very good agreement with experimental results (De Marchis & Napoli, 2008). Since in this case secondary currents play a very important role too, the weak performance of RANS approach in river confluence analysis seems to be mostly assignable to the inability to describe the interaction of two helical flows.

Miyawaki *et al.* (2009) overcame this problem using DES (Detached Eddy Simulation) to simulate the flow at the confluence of two small rivers in Illinois (USA). DES is a hybrid technique

where wall regions are resolved using the RANS approach, while Large Eddy Simulation (LES) is used elsewhere. In Large Eddy Simulation, the large scales of fluid motion are solved from the Navier-Stokes equations and a sub-grid scale (SGS) model is applied to describe the effect of the small scales on the large ones. Miyawaki *et al.* (2009) used a large number of computational cells (4.5 million cells) in order to be able to resolve the wall region without recurring to any wall law.

The discharge downstream of the confluence in the flow field analyzed by these authors was 2.75 m^3/s, with a Reynolds number close to 166,000 and a momentum ratio between the incoming discharges very close to unity. These values are much lower than in the problem analyzed in this paper, where the discharge and the Reynolds number are more than about 50 and 100 times higher, respectively. These very high values do not allow to perform a proper "resolved" LES, in which the viscous sublayer is directly resolved without using wall laws. The main aim of the numerical analysis in this paper is to investigate the ability of LES with wall models to properly reproduce the measured flow field, providing a fine description of the helical flow due to the confluence of two curved tributary channels.

The filtered Navier-Stokes and continuity equation for free surface flows

$$\frac{\partial \overline{u}_i}{\partial t} + \frac{\partial \overline{u_i u_j}}{\partial x_j} - \nu \frac{\partial^2 \overline{u}_i}{\partial x_j \partial x_j} + \frac{1}{\rho}\frac{\partial \overline{q}}{\partial x_i} + g\frac{\partial \overline{\eta}}{\partial x_i} + \frac{\partial \tau_{ij}}{\partial x_i} = 0 \quad (1)$$

$$\frac{\partial \overline{u}_i}{\partial x_j} = 0 \quad (2)$$

are resolved, where u_i (i=1,2,3) are the velocities, x_i are the coordinates (with the x_3 axis vertical and oriented upward), t is the time, g is the gravity acceleration, ρ is the water density, ν is the kinematc viscosity, $\eta(x_1,x_2)$ is the free-surface level, q is the pressure excess over hydrostatic, $\tau_{ij} = \overline{u_i u_j} - \overline{u}_i \overline{u}_j$ is the SubGrid Scale (SGS) stress tensor and the overline indicates filtered values. The PANORMUS (PArallel Numerical Open-souRce Model for Unsteady flow Simulation) code is used to resolve equations (1) and (2), whose ability to solve LES equations on curvilinear grids has been demonstrated in Napoli *et al.* (2008) and De Marchis *et al.* (in press).

Equations are discretized using a collocated finite volume method, employing curvilinear non-orthogonal structured grids consisting of non-overlapping hexahedral cells. First and second spatial derivatives are discretized using second-order accurate central formulae (the second-order accuracy of the numerical method has been demonstrated in Lipari and Napoli (2008)).

Time derivatives are calculated using an Euler scheme, providing second-order accuracy at the time level n + 1/2 (that is at time (n + 1/2) Δt, where Δt is the time step). The terms containing spatial derivatives are calculated at the time level n+1/2 using an implicit discretization of the vertical turbulent terms based on the Crank-Nicolson scheme, whereas explicitly treating the other terms by the Adams-Bashfort scheme.

In order to overcome the incompressible pressure-velocity decoupling, a fractional-step method is applied for the solution time-marching.

At each time step, the free surface elevation is recalculated according to the kinematic condition for the free-surface,

$$\frac{\partial \overline{\eta}}{\partial t} + \overline{u}_1 \frac{\partial \overline{\eta}}{\partial x_1} + \overline{u}_2 \frac{\partial \overline{\eta}}{\partial x_2} - \overline{u}_3 = 0 \quad (3)$$

which is obtained prescribing that the free-surface is a material surface. Equation (3) is discretized using central formulae as in eq. (1)-(2).

For a detailed description and validation of the numerical code, the reader is referred to Lipari & Napoli (2008).

In the present LES, the anisotropic part of the SGS stress tensor is modeled using the Smagorinsky model,

$$\tau_{ij}^{a} = -\nu_t \left(\frac{\partial \overline{u}_i}{\partial x_j} + \frac{\partial \overline{u}_j}{\partial x_i} \right) \quad (4)$$

with

$$\nu_t = (C_s \Delta)^2 |\overline{S}| \quad \text{and} \quad |\overline{S}| = (2\,\overline{S}_{ij}\overline{S}_{ij})^{1/2} \quad (5)$$

where $\Delta = (\Delta x_1\, \Delta x_2\, \Delta x_3)^{1/3}$ and the value Cs = 0.1 is used as closure coefficient. The dynamic calculation of the closure coefficient (*Dynamic Smagorinsky Model,* Germano *et al.* (1991)) has not been used since the range of resolved turbulence scales is not large enough to ensure effective use of the Germano identity.

The domain is meshed with 332 x 132 x 20 cells in the streamwise, spanwise and vertical directions, respectively. Inflow boundary conditions were obtained on both the tributary rivers using separate simulations of fully developed turbulent flows, using periodical boundary conditions in the streamwise direction. The obtained instantaneous velocity field is then used to feed the inflow sections with data having the appropriate spatial correlations. To this aim the procedure proposed by Kempf *et al.* (2005) is used.

The relatively coarse grid does not allow to directly resolve the viscous sublayer. A logarithmic wall-law is thus used to obtain the wall boundary

conditions. Null derivatives for the velocity are prescribed at the outflow boundary.

The PANORMUS code has been fully parallelized using the Message Passing Interface (MPI) paradigm. Simulations have been conducted on a cluster machine with four nodes each with two processors.

4.2 *Results*

The analysis of the results will be mostly conducted on time averaged data, with the aim to show the ability of the employed technique to adequately describe the complex flow field downstream of the river confluence. Some analysis of the instantaneous hydrodynamic field will be shown too.

The river confluence is characterized by a strong asymmetry of the tributary rivers, since the ratio of the incoming current momentum is about 1.8. Moreover, the Mosoni-Duna approaches the confluence with a slight bend, whereas the River Rába does so with a sharp bend after flowing around Radó Island (see Fig. 1). As a consequence, the latter tributary exhibits a pronounced secondary flow pattern just upstream of their merging with each other. On the contrary, secondary flow in the River Mosoni-Duna is quite weak, as it can be seen in figure 6, where the tangent velocity field in two cross sections upstream of the confluence is plotted. The figure clearly shows a clockwise-rotating streamwise-oriented vortex in the River Rába. In the River Mosoni-Duna the secondary flow pattern is much simpler, with the current relatively weakly flowing toward the right bank.

Downstream of the confluence the vortex in the River Rába is convected toward the left (close to the center of the river), while the surface high speed streamwise current is diverted downward.

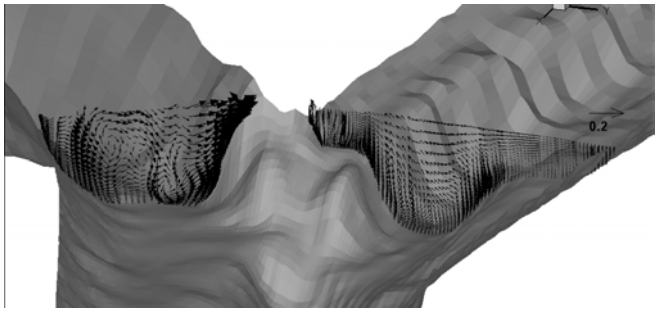

Figure 6. Secondary flow patterns in two cross-sections upstream of the confluence.

This pattern is easily identifiable in Figures 7 and 8 showing some streamlines with starting points in both the tributary branches. The streamlines after the merging rapidly deflect toward the bed. In the figures the colors indicate the height, thus clearly highlighting the downward flow. This strong downward current appears to be the main responsible for the formation of the pronounced scour hole just downstream of the confluence.The figures show that the flow coming from River Mosoni-Duna mostly contribute to the hole excavation. The streamlines with origin in the River Rába, in fact, reach lower depths before being captured by the high speed streamwise current, causing their upwelling toward the free-surface. By contrast, streamlines with origin in the Mosoni-Duna quickly drop toward the hole bottom, to be only partially captured by surface current.

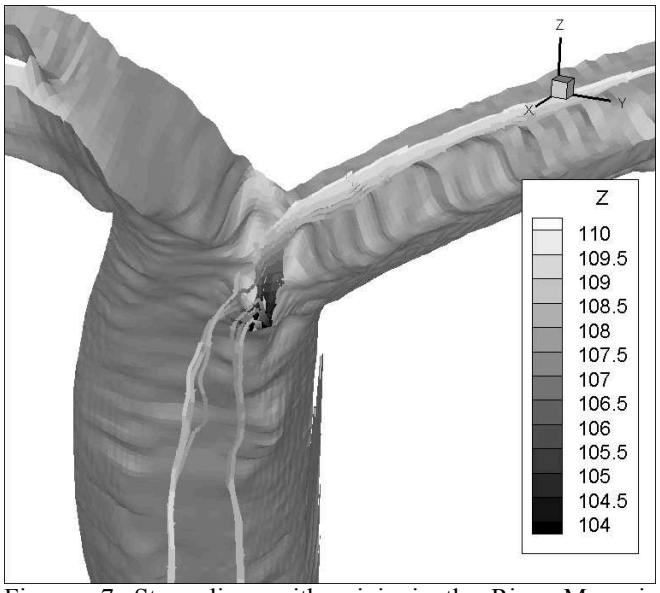

Figure 7. Streamlines with origin in the River Mosoni-Duna. Color scale indicates the height.

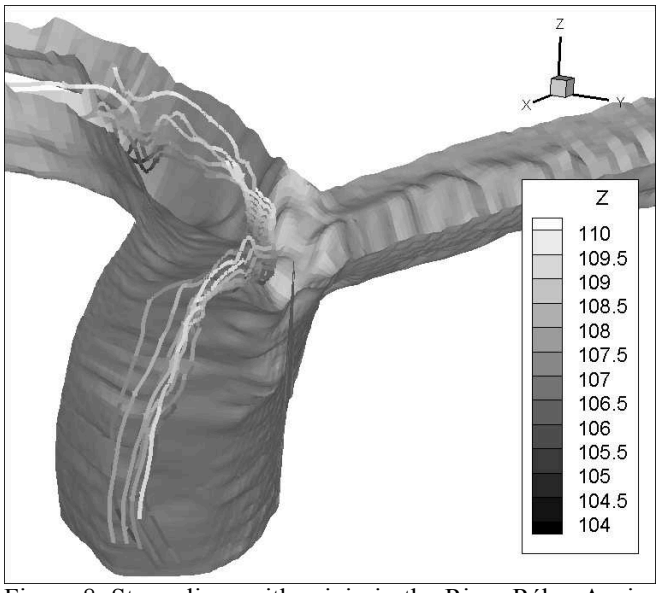

Figure 8. Streamlines with origin in the River Rába. Again, color scale indicates the height.

Further insight into the complex flow pattern can be obtained through the analysis of streamwise velocity contour-lines in some cross-sections just upstream and downstream of the confluence. In Figure 9a the velocity distribution is shown in two cross-sections upstream of the confluence. As noticed above, the flow current in the River Rába

is quite stronger than in the River Mosoni-Duna. Moreover, the strong secondary flow in the former branch causes the formation of a zone of high velocity extending toward the bottom, with the maximum at the mid-depth instead than at the free-surface. Comparison of the velocity distributions in Figures 9b and 9c then highlights the important role of the scour hole in the tributary flow merging. In correspondence of the scour hole (Fig. 9b), in fact, the velocity distribution has still one maximum on the River Rába side, while just downstream of it (Fig. 9c), two maxima can be clearly identified. A strong mixing thus occurs in that region, that some tenth of meters downstream (Fig. 9d) results in an almost complete mixing. The results shown in Figures 9a-d are in good agreement with the spatial velocity distribution obtained from moving boat ADCP measurements. Some velocity over-prediction in the River Mosoni-Duna can be seen, which is probably due to a slightly too large imposed discharge in that branch in numerical simulations, as obtained from cross-section integration of experimental data.

LES results allow identifying flow structures that cannot be displayed when analyzing Reynolds-averaged hydrodynamic fields. Specifically, the instantaneous vertical vorticity field at the free surface in the wake region downstream of the confluence, plotted in figure 10, provides important insights in the mixing process. The figure shows patterns somewhat analogous to the typical mixing-layer vorticity structure. Nevertheless, since the much higher flow complexity with respect to the "simple" mixing-layer phenomenon (due to the bed configuration, the presence of bends upstream of the merging, and the angle of incidence of the tributaries), vortical structures are much less regular than one would expect in that case. In the wake region downstream of the confluence, an alternating pattern of positive and negative almost isotropic (in the horizontal plane) vorticity areas develops. This zone extends for about 50 m. Then, the coherent structures assume a progressively elongated shape, while being characterized by an undulating pattern. Finally, at about 200 m downwind of the confluence, the vorticity regions are even more elongated and definitely streamwise oriented. These vorticity areas far from the confluence are mostly driven by the bottom morphology. Moreover, an high vorticity (mostly positive) area develops close to the left bank of the river after the confluence, clearly due to the flow separation caused by the submerged spike easily identifiable in figure 1, showing the bottom topography of the analyzed area.

5 CONCLUSIONS

The flow structures at a confluence zone of two moderate size rivers were investigated by several tools. Moving boat and stationary ADCP measurements offered on one hand an overall, though locally instantaneous, spatial velocity field, and local time-averaged velocity profiles, on the other. Helical flow structures of the confluence zone were shown by representing secondary current strengths and orientation in a vector form. 3D RANS type of modeling could be validated to reproduce the essentials of the spatial flow structure. Furthermore, successful attempts were made to capture the space-time behavior also on a LES modeling-basis, focusing on the reasonable reproduction of the rather complex vortical motion in the post-confluence channel reach, as a possible combination of vortex shedding at the blunt tip of the confluence and shear layer instabilities turning to Kelvin-Helmholtz type of vortex formation at the interface zone of the two rivers, all this besides the developing helical flow components.

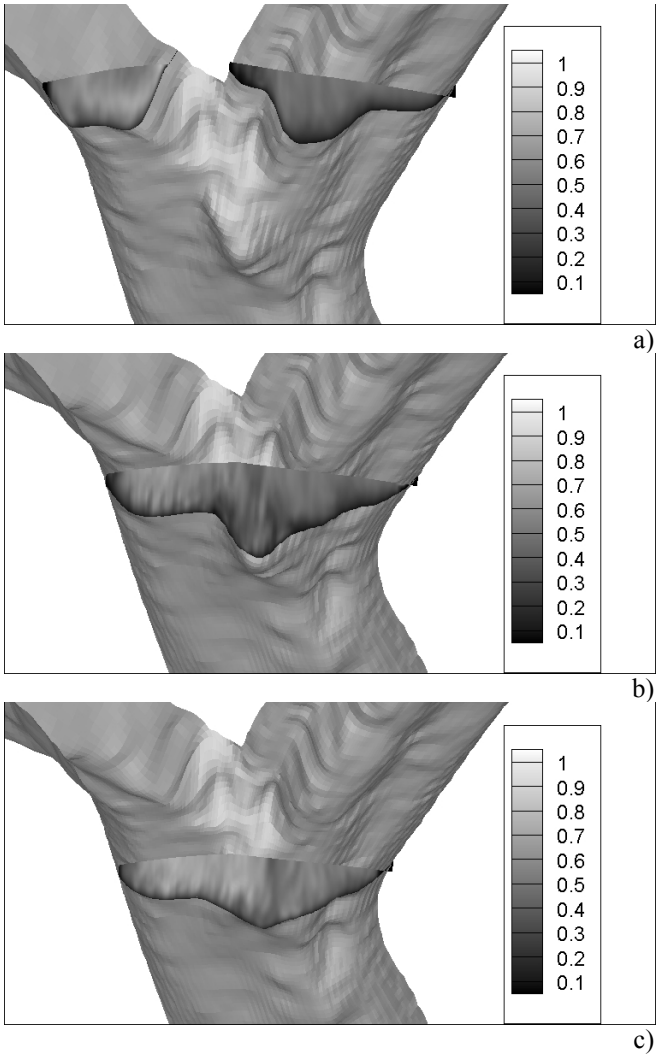

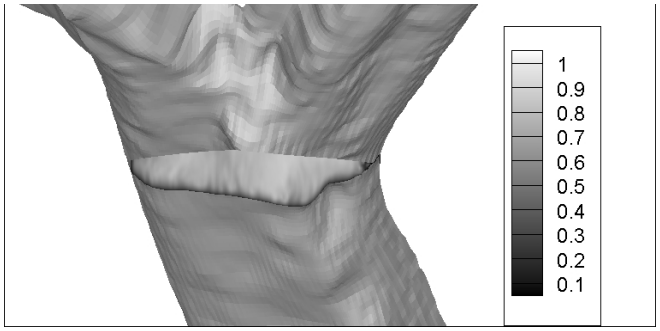

d)

Figure 9. Contour-lines of the streamwise velocity distribution in four cross-sections upstream and downstream of the confluence.

REFERENCES

Biron, P. M., Ramamurthy, A. S. and Han, S. 2004. Three-Dimensional Numerical Modeling of Mixing at River Confluences., Journal of Hydraulic Engineering, vol. 130, 243-253.

Bradbrook, K. F., Lane, S. N., Richards, K. S., Biron, P. M. and Roy, A. G. 2000. Large Eddy Simulation of periodic flow characteristics at river channel confluences. Journal of Hydraulic Research, vol. 38, 207-216.

De Marchis, M., Napoli, E., 2008. The Effect of Geometrical Parameters on the Discharge Capacity Of Meandering Compound Channels. Adv. Water Res., Vol. 31 (12), pp. 1662-1673.

De Marchis, M., Napoli, E., Armenio, V., in press. Turbulence structures over irregular rough surfaces, J TURBULENCE.

De Serres, B., Roy, A. G., Biron, P. M. and Best, J. L., 1999.Three-dimensional structure of flow at a confluence of river channels with discordant beds. Geomorphology, vol. 26, 313-335.

Germano, G., Piomelli, U., Moin, P., Cabot, W.H., 1991. A dynamic subgrid-scale eddy viscosity model. Phys. Fluids A 3, p. 1760-1769.

Kempf, A., Klein, M., Janicka, J., 2005. Efficient Generation of Initial- and Inflow-Conditions for Transient Turbulent Flows in Arbitrary Geometries. J FLOW TURB COM, Vol. 74 (1), pp. 67-84.

Lipari, G., Napoli, E., 2008. The impacts of the ALE and hydrostatic-pressure approaches on the energy budget of unsteady free-surface flows. COMP FLUIDS, vol. 37, pp. 656-673, ISSN: 0045-7930.

Miyawaki, S., Constantinescu, G., Kirkil, G., Rhoads, R., Sukhodolov, A., 2009. Numerical Investigation of Three-Dimensional Flow Structure at a River Confluence. Proceedings of the 33rd IAHR Congress: Water Engineering for a Sustainable Environment, Vancouver, Canada.

Napoli, E., Armenio, V., De Marchis, M., 2008. The effect of the slope of irregularly distributed roughness elements on turbulent wall-bounded flows. J FLUID MECH, Vol. 613, pp. 385-394.

Olsen, N. R. B. 2002. A three-dimensional numerical model for simulation of sediment movements in water intakes with moving option. User's Manual, Department of Hydraulic and Environmental Engineering, The Norwegian University of Science and Technology, Trondheim, Norway.

Patankar, S. V. 1980. Numerical heat transfer and fluid flow. McGraw-Hill Book Company, New York.

Pope, S. B. (2001), Turbulent Flows. Cambridge University Press.

Rhoads, B. L. and Sukhodolov, A. N., 2001a. .Field Investigation of Three-Dimensional Flow Structure at Stream Confluences: 1. Thermal Mixing and Time-Averaged Velocities., Water Resour. Res., vol. 37, 2393-2410.

Rhoads, B. L. and Sukhodolov, A. N., 2001b. .Field Investigation of Three-Dimensional Flow Structure at Stream Confluences: 2. Turbulence., Water Resour. Res., vol. 37, 2411-2424.

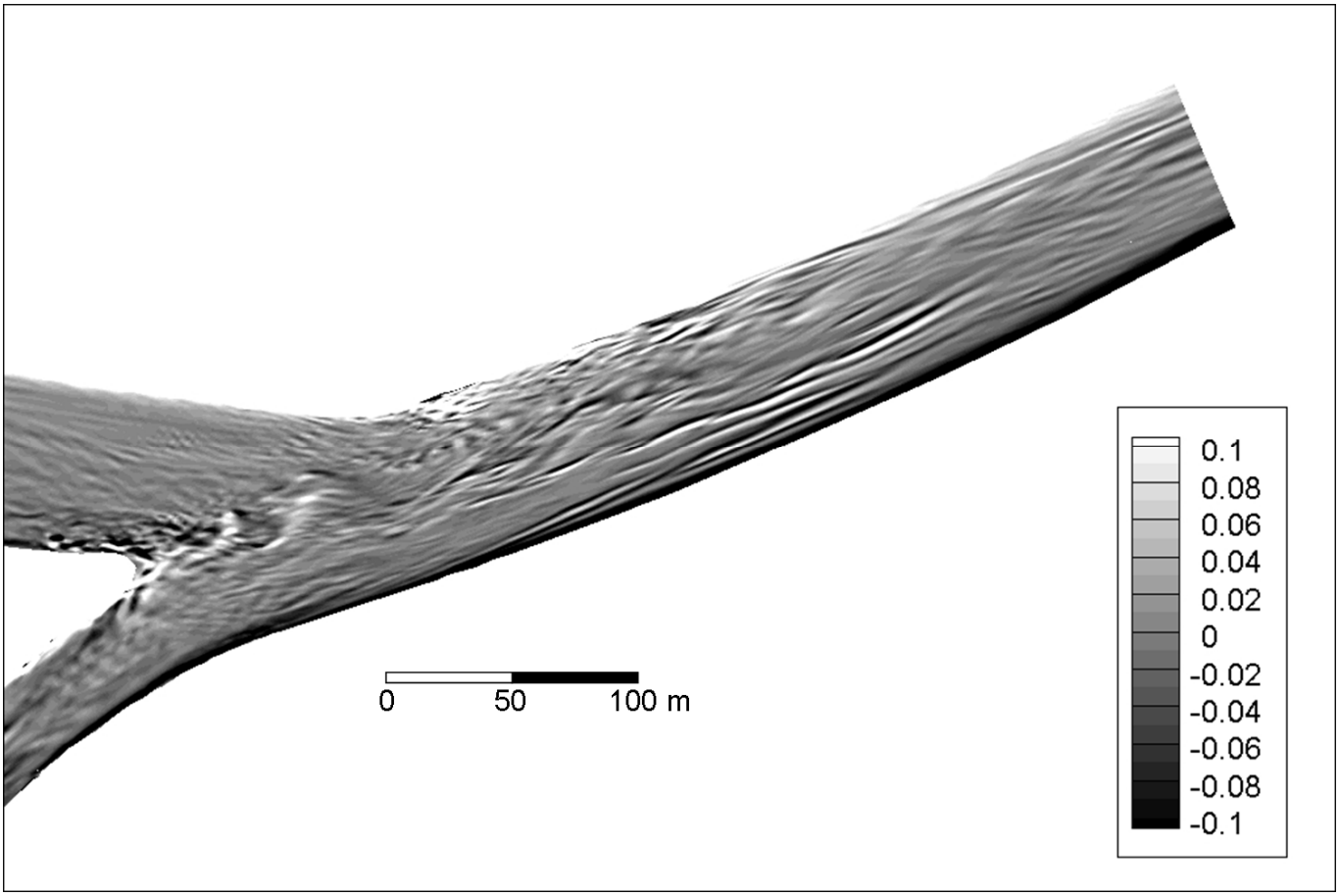

Figure 10. Instantaneous vertical vorticity distribution at the free-surface